Source coherence impairments in a direct detection direct sequence optical code-division multiple-access system

Ihsan Fsaifes, Catherine Lepers, Mounia Lourdiane, Philippe Gallion, Vincent Beugin, and Philippe Guignard

We demonstrate that direct sequence optical code-division multiple-access (DS-OCDMA) encoders and decoders using sampled fiber Bragg gratings (S-FBGs) behave as multipath interferometers. In that case, chip pulses of the prime sequence codes generated by spreading in time-coherent data pulses can result from multiple reflections in the interferometers that can superimpose within a chip time duration. We show that the autocorrelation function has to be considered as the sum of complex amplitudes of the combined chip as the laser source coherence time is much greater than the integration time of the photodetector. To reduce the sensitivity of the DS-OCDMA system to the coherence time of the laser source, we analyze the use of sparse and nonperiodic quadratic congruence and extended quadratic congruence codes. © 2007 Optical Society of America

OCIS codes: 060.2340, 0604510.

1. Introduction

The growth of new communication services (e.g., data and video) has increased the demand for high-speed and large capacity communications in access networks. Optical fiber support is an answer to face this demand, but its deployment is slowed down by the current highly competitive environment. Among the different scenarios to decrease investment costs, solutions sharing a network between several users or services are often put forward by telecommunication operators. For this purpose, several multiple access schemes have been studied such as wavelength division multiplexing (WDM), optical time-division multiplexing (OTDM), or hybrid approaches. These approaches have been extensively explored and used in optical communication systems. A great deal of attention has recently been paid to the optical code-division multiple-access (OCDMA) technique. This technique offers an all-optical encoding–decoding processing using optical devices and a large number of users with asynchronous access capability.[1]

OCDMA techniques can be classified by following two criteria: on the working principle, i.e., OCDMA coding can be incoherent when coding is done on an optical power basis[2] or can be coherent when the coding is done on a complex amplitude basis[3,4]; on the coding dimension, i.e., OCDMA coding can be performed either in the time or the frequency domain, or in the time and frequency domains simultaneously. In the time domain, each user data bit is encoded with a given sequence of pulses referred to as chips. The bits are then broadcast onto the network and are decoded with the matched specific user code.[5] In the frequency domain, the total source bandwidth is divided into several subbands, and the different central carrier frequencies are selected to compose a well-defined code sequence that can once again be suitably identified by a matched optical decoder.[6] Other coding domains such as space and polarization domains have also been studied.[7–9]

The performances of OCDMA systems are related to the correlation properties of the used code families. Previous work on direct sequence (DS)-OCDMA was presented using optical orthogonal codes (OOCs) and prime sequences (PSs). OOCs have been reported to achieve good correlation properties, i.e., high autocorrelation main peak and low cross-correlation function

I. Fsaifes (fsaifes@enst.fr), M. Lourdiane, and P. Gallion are with the Ecole Nationale Supérieure des Télécommunications (GET Télécom Paris), Centre National de la Recherche Scientifique, Unité Mixte de Recherche 5141, 46 rue Barrault, 75013 Paris, France. C. Lepers and V. Beugin are with the Laboratoire de Physique des Lasers, Atomes et Molécules, Centre National de la Recherche Scientifique, Unité Mixte de Recherche 8523, Université de Lille I, 59650 Villeneuve d'Ascq, France. P. Guignard is with the Division Recherche et Développement, France Télécom, 2 avenue Pierre Marzin, 22307 Lannion, France.

Received 7 July 2006; accepted 8 September 2006; posted 21 September 2006 (Doc. ID 72772); published 17 January 2007.
0003-6935/07/040456-07$15.00/0

lobes to reduce undesired interferences with other users referred to as multiple-access interference (MAI).[10,11] PSs have been shown to improve the multiplexing capacity for a given code length while relaxing the OOC autocorrelation function constraints.[12,13]

The key components of OCDMA systems are the encoder–decoder that performs code generation and data recognition. The earliest implementation of an all-optical CDMA system was performed using optical delay lines for CDMA time-domain coding. By injecting an optical pulse into the different optical delay lines, a series of pulses is generated depending on a given chip sequence. In the past few years, fiber Bragg gratings (FBGs) have been used to implement the encoder–decoder for OCDMA applications. FBGs are passive spectral filters and offer significant advantages such as ready integrability with all fiber-optic systems, compactness, and low fabrication cost.

Different types of FBG have been used such as moiré FBGs for wavelength-temporal encoding, arrays of uniform FBGs for wavelength encoding (frequency hopping OCDMA) and chirped FBGs for phase encoding. Sampled fiber Bragg gratings (S-FBGs) are used for temporal encoding (DS-OCDMA).[14–17]

Until now, many studies on OCDMA systems have been performed with incoherent sources, and in that case, the autocorrelation function is considered as the sum of optical powers of all chip pulses to be combined.[18,19] However, an ideal incoherent source with zero coherence time would require infinite bandwidth, which is impossible. It is interesting to study how OCDMA systems operate with a practical light source. The effect of beat noise and the spectral efficiency in coherent and incoherent time-spreading OCDMA have recently been studied.[20–22]

Here we analyze the correlation properties of a direct detection DS-OCDMA using a coherent laser source. PS codes are generated by spreading in time-coherent data pulses from a 1551 nm distributed feedback (DFB) laser with an integrated electroabsorption modulator. The generated pulse width equal to the chip time duration ($T_p = T_c = 50$ ps) and the integration time of the detector ($T_D = 100$ ps) are very small compared with the coherence time of the DFB laser $\tau_c = 1\ \mu$s. Owing to S-FBG technology, encoders and decoders behave as multipath interferometers. In those conditions, the generated primary and secondary pulses of the code sequences remain correlated and interfere as they superimpose within a chip time duration. The resulting autocorrelation function is then the sum of the complex amplitudes of the combined chip pulses of the periodic PS codes considered here. To minimize superimposition of the chip pulses, nonperiodic, sparser and longer QC and EQC codes are suggested and studied.[23–25] Simulations performed on these codes demonstrate that the autocorrelation function is less sensitive to interferometric perturbations.

In Section 2 we introduce the correlation properties of the PS code family. The design and realization of two periodic S-FBGs of PS code family encoders–decoders are reported. In Section 3 we analyze the influence of the coherence time of the laser source on the correlation performances of PS codes in a DS-OCDMA system. We analyze the technological constraints that lead to multipath interferometer behavior of the DS-OCDMA devices. We demonstrate the mechanisms of code sequence generation and autocorrelation function construction in the presence of optical interferences. In Section 4 we carry out correlation property comparisons of QC, EQC, and PS codes. We design the corresponding QC and EQC DS-OCDMA encoders and decoders with S-FBG technology, and we simulate the temporal responses of such devices. Finally, we provide some useful discussions and conclusions.

2. Performances of Prime Sequence Codes with Sampled Fiber Bragg Gratings

In DS-OCDMA systems, each user data bit is encoded by unipolar pulses also called chips. As the information is not phase encoded, direct detection is used. PS sequence codes are revealed to be interesting codes to implement because of their good user multiplexing capacity as compared with OOCs. In this section, we will briefly underline their correlation properties, then we will describe the design and the realization of periodic PS encoders–decoders with S-FBGs.

A. Auto-Cross-Correlation Properties of Prime Sequences

The PS codes considered here exhibit quasi-orthogonal properties. Autocorrelation and cross-correlation functions AC_m and $CC_{m,n}$ are given by

$$AC_m(s) = \sum_{i=0}^{L-1} C_m(i)C_m(i-s)\begin{cases} =\omega & \text{for } s = 0 \\ \leq \lambda_a & \text{for } 1 \leq s < L' \end{cases}$$

$$CC_{m,n}(s) = \sum_{i=0}^{L-1} C_m(i)C_n(i-s) \leq \lambda_c \quad \text{for } 0 \leq s < L, \tag{1}$$

where C_m and C_n are two different code sequences, and λ_a and λ_c are, respectively, the maximum autocorrelation and cross-correlation levels. The weight of sequence ω is the number of chips equal to 1 in a given code sequence and is equal to user multiplexing capacity. L denotes the sequence length.

The selected code sequences of the experiment are PS codes generated from prime number $p = 3$ ($\omega = 3, L = 9$). We chose to design and to develop periodic PS codes C_1 (100010001) and C_2 (100100100) by implementation of S-FBGs devices. A periodic code sequence has the same 0 chip number between two successive 1 chips. The behavior of periodic code sequences is more sensitive to interferometric effects than the nonperiodic code C_3 (100001010) as we will see hereafter.

B. Sample Fiber Bragg Grating Encoder–Decoder Design

Code words are implemented by using S-FBGs reflecting a 50 ps user pulse train (Fig. 1). Each 1 chip is reflected by a FBG, and an optical fiber length (ΔL)

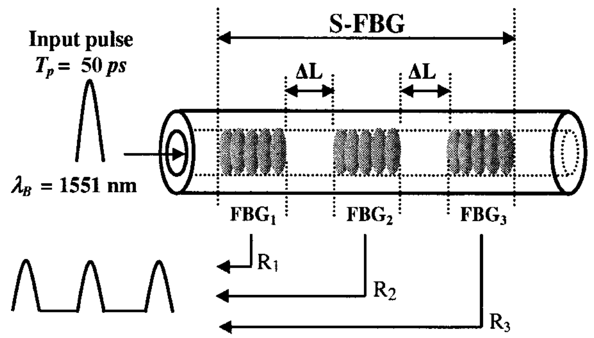

Fig. 1. S-FBG design for encoding–decoding of user data bits.

between two successive FBGs represents the number of 0 chips.

C_1 and C_2 code sequences are generated from S-FBG^1 (FBG$_1^1$, FBG$_2^1$, FBG$_3^1$) and S-FBG^2 (FBG$_1^2$, FBG$_2^2$, FBG$_3^2$) devices at a 1551 nm Bragg wavelength. Reflectivity R_j of the FBG$_{j=1,2,3}^i$ of the C_i encoder device is, respectively, 16% (j = 1), 24% (j = 2), and 34% (j = 3). In the case of the C_1 encoder, a 21,500 μm fiber length proportional to $3T_c$ time duration separates two successive FBGs. For the C_2 encoder, the fiber length is 15,500 μm, which is proportional to a $2T_c$ time duration.

It is worth noting that the distances separating the different FBG$_j^i$ are larger than the pulse spatial length (approximately 10,000 μm), which avoids overlap between successive data pulses. Furthermore, the spectral width of the input pulse (20 GHz) is significantly lower than the width of the FBG photonic bandgaps (>100 GHz). This implies that the group velocity dispersion introduced by each Bragg grating is not significant as long as the laser wavelength is tuned to the Bragg wavelength.

The optimization of the refractive index modulation depth for each FBG allows compensation of optical power depletion of the input pulse caused by partial reflections from the FBGs. Accordingly, in the case of an incoherent source, it should lead to generate reflected pulses with approximately similar mean optical power.

C. Sampled Fiber Bragg Grating Encoder–Decoder Realization

Encoder–decoder technological realization is achieved by UV photoinscription of in-fiber Bragg gratings with the phase mask method.[26] To fulfill the device specifications, an optimized technological fabrication process has been developed. In the first step of each device realization, a uniform 500 μm long FBG$_3$ (grating with the highest reflectivity R_3 = 34%) was written in a H_2-loaded SMF 28 fiber by exposing a phase mask to UV pulses from a KrF laser at 248 nm. The phase mask pitch was Λ = 1071.6 nm, which permitted us to obtain a Bragg wavelength resonance at 1551 nm.

During this inscription, the evolution of the grating reflectivity was recorded as a function of the number of writing pulses (N_i) to get a useful calibration curve of R_j growth for the following inscriptions. All the exposures were carried out at a frequency rate of 20 Hz, and a mean fluence per pulse of F_p = 160 mJ/cm^2 ± 20 mJ/cm^2.

The second step is to move the fiber along its axis over a length corresponding to the required 0 chips and then in writing the next grating (FBG$_2$, R_2 = 24%). The control of the FBG$_2$ inscription was achieved thanks to the previously recorded curve. The third grating (FBG$_1$, R_1 = 16%) was then written following a similar process. To accurately control the fiber length separating two consecutive FBGs, the fiber was mounted on a piezotranslation stage controlled with an interferometric rule.

3. Source Coherence Time Influence on the Autocorrelation Function Shape

Here we show that the shape of the autocorrelation function depends on device and system features.

A. Influence of the Sampled Fiber Bragg Grating Device Characteristics

Fiber lengths ΔL limited with FBGs inside an encoder–decoder act as coupled Fabry–Perot cavities. We have observed by simulation that a λ_B-order variation of ΔL induces phase differences ($\Delta\varphi = 2\pi \Delta L/\lambda_B$) on the reflected optical pulses and contributes to modify the shape of the temporal response and consequently of the reconstructed autocorrelation function. It confirms that the DS-OCDMA system behaves as a multipath interferometer.

We have also shown that, as FBGs inside the same device are centered at different Bragg wavelengths, a modulation of the reflectivity of encoder–decoder versus wavelength occurs.[27] Consequently, the reflected optical powers of the code pulses depend on laser source wavelength drift. This effect coexists with interferometric effects. To observe the latter, we will take care to stabilize the laser source.

Furthermore, the encoder and the decoder can take different mean Bragg wavelengths. As a practical solution, we let the encoder–decoder operate at the same mean Bragg wavelength by tuning the wave-

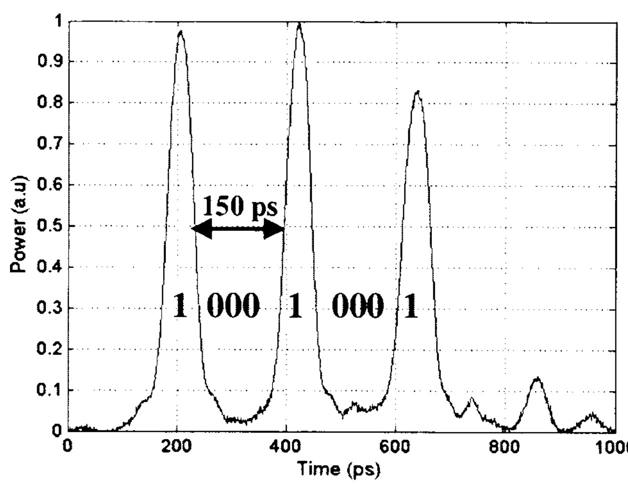

Fig. 2. Experimental time response of a S-FBG^1 encoder.

length of the decoder with a stretching system. To avoid additional wavelength thermal drift, the encoder and the decoder are also protected within an appropriate package.[28,29]

B. Influence of the Characteristics of the System

Since the DFB laser source coherence time τ_c (1 μs) of the system is much greater than the chip time duration T_C (50 ps) and the integration time of the photodetector T_D (100 ps), the encoded pulses remain phase correlated. Furthermore, the encoder and the decoder act as multipath interferometers as the different FBGs behave like partial couplers of three coupled Fabry–Perot cavities. In those conditions, destructive or constructive optical interferences may occur in the OCDMA system as pulses from different paths in the interferometer superimpose within the chip time duration. A typical experimental temporal response of encoder C_1 is displayed in Fig. 2. The two first pulses have the same optical power, but the third one gets lower optical power.

In the third pulse of the code sequence, coherent interactions appear between the pulses resulting from primary reflection from FBG_3 and secondary reflection from the Fabry–Perot cavity limited by FBG_1 and FBG_2. In Fig. 2, the primary and secondary pulses interfere destructively within the chip time duration.

Let the optical power P be incident on the encoder device and the optical powers P_1, P_2, and P_3 be reflected from FBG_1, FBG_2, and FBG_3, respectively,

$$P_1 = R_1 P,$$

$$P_2 = (1 - R_1)^2 R_2 P,$$

$$P_3 = (1 - R_1)^2 (1 - R_2)^2 R_3 P. \tag{2}$$

The interaction between the electric fields associated with the reflected optical powers P_3 and P_3'' of the secondary reflected pulse due to the Fabry–Perot cavity limited by FBG_1 and FBG_2 within the chip time duration leads to a third pulse whose optical power is

$$P_3' = P_3 + P_3'' + 2\sqrt{P_3 P_3''}\cos(\Delta\Phi),$$

$$P\,''_3 = (1 - R_1)^2 R_1 R_2{}^2 P. \tag{3}$$

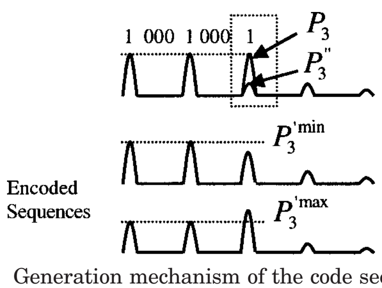

Fig. 3. Generation mechanism of the code sequence.

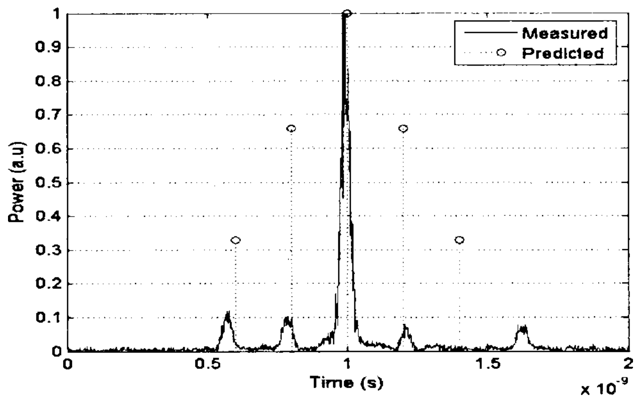

Fig. 4. Predicted (dotted line) and experimental (solid curve) autocorrelation functions obtained with a matched decoder, i.e., $C_1 * C_1$.

Depending on the $\Delta\Phi$ value and the polarization conditions, the third pulse of the code can take different optical power levels between two extrema values $P_3'^{\max}$ and $P_3'^{\min}$:

$$P_3'^{\max} = P_3 + P_3'' + 2\sqrt{P_3 P_3''}$$

$$P_3'^{\min} = P_3 + P_3'' - 2\sqrt{P_3 P_3''}. \tag{4}$$

The mechanism of the generation of the code sequence is illustrated in Fig. 3.

Let us note that the first and second pulses of the code are not affected by multiple reflected pulses. Their optical power remains constant while the DFB laser wavelength is stable and tuned to the mean Bragg wavelength of the encoder.

The experimental decoding of the C_1 encoded pulse sequence by the matched device S-FBG[1] in a single user configuration is shown in Fig. 4. The reconstructed autocorrelation function was obtained by carefully controlling the polarization state of the light in the OCDMA system to get the best autocorrelation shape. This function has a maximum optical power peak and sidelobes whose optical power is very low (approximately 10% of the maximum peak). We should expect first sidelobes with optical power equal to $\frac{2}{3}$ of the main peak optical power. The second side

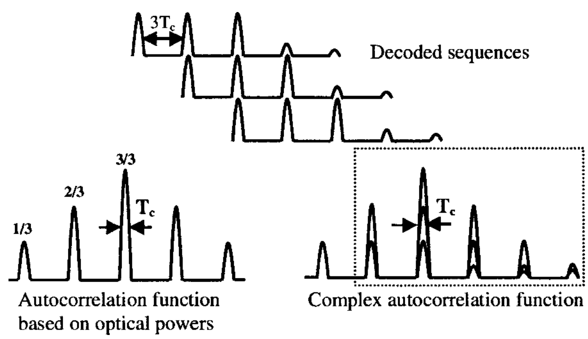

Fig. 5. Construction mechanism of the autocorrelation function.

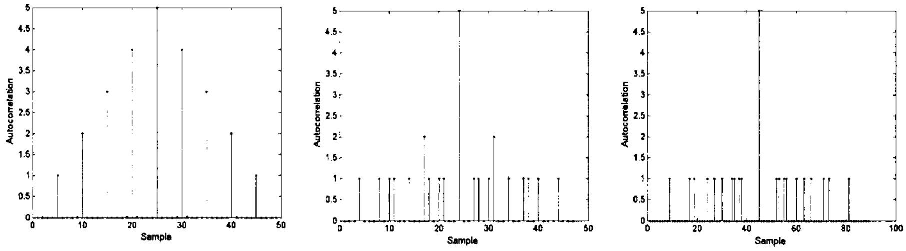

Fig. 6. Autocorrelation functions of PS, QC, and EQC codes, respectively, with $p = 5$.

lobes should be equal to $\frac{1}{3}$ of the main peak optical power.

In fact, during the decoding process, each of the three main pulses of the code sequence generates the same pulse sequence. The three resulting generated sequences are delayed from each other by a $3T_c$ time duration. The interferences between superimposed pulses occur during the reconstruction of the encoded initial pulse (Fig. 5). In those conditions, taking into account the coherence time of the laser source in a DS-OCDMA system leads to a complex autocorrelation function. This behavior of the system can affect its performances and can result in a bit error rate penalty.[30]

4. Correlation Property Analysis of Quadratic Congruence and Extended Quadratic Congruence Nonperiodic Codes

To improve the functionality of the OCDMA system in an access network context, one solution is to lower the coherence time of the light source. We suggest the use of nonperiodic code sequences such as the so-called QC and EQC code families to get code sequences and an autocorrelation function less sensitive to interferometric perturbations.

Here we give the characteristics of QC and EQC codes and compare their correlation properties with those of PS. QC and EQC code specifications are reported by using FBG technology. In conclusion, correlation performances are presented.

A. Comparison of Correlation Properties of Prime Sequences, Quadratic Congruence, and Extended Quadratic Congruence Codes

Here we compare correlation properties of PS, QC, and EQC codes. To perform this comparison, we take into account optical power summation. It is noticeable that the out-of-phase sidelobes of the PS autocorrelation function can be as high as p-1 while the QC and the EQC codes have been designed to avoid these high autocorrelation sidelobes. They take a maximum value of $\lambda_a = 2$ for QC and $\lambda_a = 1$ for EQC. The cross-correlation peaks take a value of $\lambda_c = 4$ for the QC in the worst case (when $p > 7$). They are limited to a maximum value of $\lambda_c = 2$ for the EQC as well as for the PS codes (Figs. 6 and 7). Let us note also that the QC and the EQC codes can ideally operate in asynchronous and synchronous modes whereas PS codes present better behavior in the asynchronous mode.

The main properties of PS, QC, and EQC codes are shown in Table 1. The main disadvantage of EQC codes is that their length is almost twice that for PS and QC codes, i.e., $p(2p - 1)$ whereas the QC code length is p^2 as is the PS one. The EQC maximum data rate per user will be reduced to almost one half of the QC and the PS data rate. However, this data rate is still interesting to be considered for access network purposes.

The main property of QC and EQC codes of interest here is their nonperiodicity, i.e., the distance between 1 chips is never the same. It leads to an all-optical

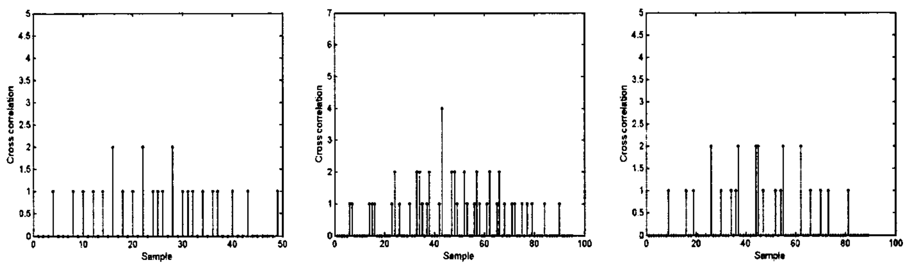

Fig. 7. Cross-correlation functions of PS, QC, and EQC codes, respectively, with $p = 7$.

Table 1. Comparison of PS, QC, and EQC Codes

Code	Length L	Weight ω	Number of Users N	λ_a	λ_c	L/ω	Code Density	CDMA System Type
PS	p^2	P	P	$p - 1$	2	P	1/2	Asynchronous
QC	p^2	P	$p - 1$	2	4	P	1/2	Synchronous–Asynchronous
EQC	$p(2p - 1)$	P	$p - 1$	1	2	$2p - 1$	$p/2(2p - 1)$	Synchronous–Asynchronous

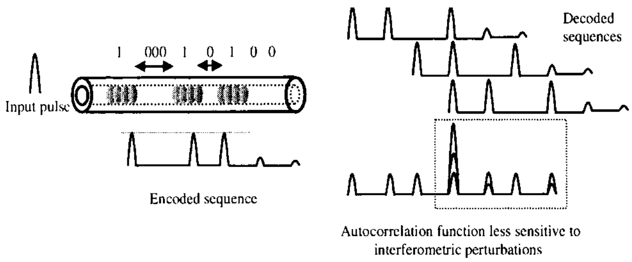

Fig. 8. Code generation and autocorrelation function reconstruction mechanisms for nonperiodic QC code ($p = 3$).

CDMA system less sensitive to interferometric effects. The multiple reflections from the FBGs of the different coupled cavities do not sum together with the main pulses in the encoder as is observed for periodic codes: This leads to code pulses with constant optical power. However, at the decoder, the different pulse trains generated from each code pulse may interfere constructively or destructively. Nevertheless, we observed that the left sidelobes are insensitive to optical interference (Fig. 8).

B. Quadratic Congruence and Extended Quadratic Congruence Specifications and Simulations

The code specifications of nonperiodic QC and EQC codes for $p = 5$ are given in Table 2. To obtain code sequences with pulses of approximately the same mean optical power, we calculated the reflectivities of each FBG by respecting the condition

$$P_1 = P_2 = P_3 = P_4 = P_5, \tag{5}$$

where $P_{1,\ldots,5}$ are the reflected optical powers from different FBGs. This optimization gives mean reflected optical power equal to 10% of the mean source input optical power. In the system simulation, the operating wavelength λ_0 of the DFB laser source is 1551 nm. The FWHM of the user pulse train is set to 50 ps.

We perform simulations for the decoding operation at the receiver, taking into account the complex amplitude of the electric field rather than the optical power. The simulations of the QC and the EQC codes for $p = 5$ are shown in Figs. 9 and 10. For both types of code, the main peaks of the autocorrelation functions are surrounded by weak sidelobes. As we consider the optical phase of the electric field, interferometric perturbations between pulses occur. As expected, the secondary sidelobes on the left side of the autocorrelation peak are not correlated with other pulses. On the right side, very low powerful sidelobes can be observed. This feature is attributed to interactions between pulses.

Some interactions attributed to the system coherence still exist but are less critical in comparison with PS codes. Further simulations show that the main autocorrelation reconstructed pulse always remains centered and is not affected by destructive interferences.

Table 2. FBG Specifications for QC and EQC Codes

	FBG_1	FBG_2	FBG_3	FBG_4	FBG_5
R_i	10%	12%	16%	23%	38%
L_i			500 μm		

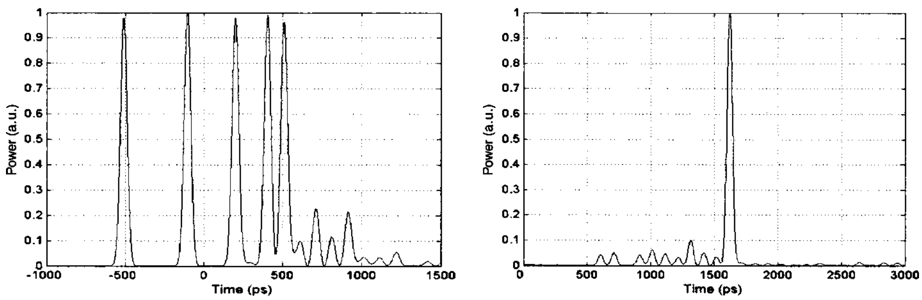

Fig. 9. Temporal response and autocorrelation function simulations for QC code (1000000010000001000101) when $p = 5$ using FBGs.

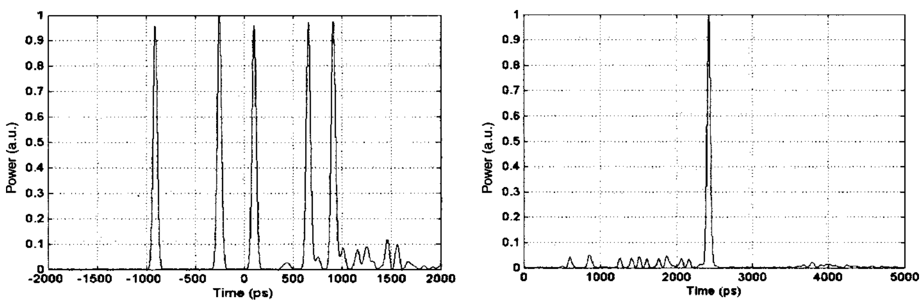

Fig. 10. Temporal response and autocorrelation function simulations for EQC code (100000000000010000001000000000010000100000000) when $p = 5$ using FBGs.

5. Conclusion

We have pointed out that the coherence time of the laser source may have an important impact on the correlation properties of a DS-OCDMA system. As this time is greater than the integration time of the photodetector, optical interferences between pulses have to be considered. We have shown that DS-OCDMA encoders and decoders based on S-FBGs behave spuriously as multipath interferometers. According to the phase and the polarization conditions, different reflected pulses may then interfere at the detection when they superimpose within a chip time duration. We have demonstrated that a complex amplitude autocorrelation function has to be considered.

This feature is not suitable in a passive optical network context as it will impact on BER performances. To overcome the sensitivity of the system to source coherence time impairments, we have suggested the use of nonperiodic QC and EQC codes, which are sparser and longer than PS codes. We have shown that the shape of the autocorrelation function is then less sensitive to interferometric effects because of the lower autocorrelation λ_a level of the QC and the EQC codes. The technological implementation of QC and EQC encoders–decoders for a DS-OCDMA application will be presented in the near future.

References

1. J. A. Salehi, "Code division multiple-access techniques in optical fiber networks. I. Fundamental principles," IEEE Trans. Commun. **37,** 824–833 (1989).
2. P. Prucnal, M. Santoro, and T. Fan, "Spread spectrum fiber-optic local area network using optical processing," J. Lightwave Technol. **4,** 547–554 (1986).
3. J. A. Salehi, A. M. Weiner, and J. P. Heritage, "Coherent ultrashort light pulse code division multiple-access communication systems," J. Lightwave Technol. **8,** 478–491 (1990).
4. N. Wada and K. Kitayama, "A 10 Gb/s optical code division multiplexing using 8-chip optical bipolar code and coherent detection," J. Lightwave Technol. **17,** 1758–1765 (1999).
5. G. E. Town, K. Chan, and G. Yoffe, "Design and performance of high-speed optical pulse-code generators using optical fiber Bragg gratings," IEEE J. Sel. Top. Quantum Electron. **5,** 1325–1331 (1999).
6. M. Kavehrad and D. Zaccarin, "Optical code-division-multiplexed systems based on spectral encoding of noncoherent sources," J. Lightwave Technol. **13,** 534–545 (1995).
7. A. A. Hassan, J. E. Hershey, and N. A. Riza, "Spatial optical OCDMA," IEEE J. Sel. Areas Commun. **13,** 609–613 (1995).
8. J. A. Salehi and E. G. Paek, "Holographic CDMA," IEEE Trans. Commun. **43,** 2434–2438 (1995).
9. J. E. McGeehan, S. M. R. M. Nezam, P. Saghari, A. E. Willner, R. Omrani, and P. V. Kumar, "Experimental demonstration of OCDMA transmission using a three-dimensional (time-wavelength-polarization) codeset," J. Lightwave Technol. **23,** 3282–3289 (2005).
10. A. Keshavarzian and J. A. Salehi, "Optical orthogonal code: acquisition in fiber optic CDMA system via the simple serial search method," IEEE Trans. Commun. **50,** 473–483 (2002).
11. Y. Chang, R. Fuji-Hara, and Y. Miao, "Combinatorial constructions of optimal optical orthogonal codes with weight 4," IEEE Trans. Inf. Theory. **49,** 1283–1292 (2003).
12. J. G. Zhang and G. Picchi, "Tunable prime code encoder/decoder for all optical CDMA applications," Electron. Lett. **29,** 1211–1212 (1993).
13. G.-C. Yang and W. C. Kwong, *Prime Codes with Applications to CDMA Optical and Wireless Networks,* Mobile Communications Series (Artech House, 2002).
14. L. R. Chen and P. W. E. Smith, "Demonstration of incoherent wavelength-encoding/time-spreading optical CDMA using chirped moiré gratings," IEEE Photon. Technol. Lett. **12,** 1281–1283 (2000).
15. P. C. Teh, P. Petropoulos, M. Ibsen, and D. J. Richardson, "A comparative study of the performance of seven- and 63-chip optical code-division multiple-access encoders and decoders based on superstructured fiber Bragg gratings," J. Lightwave Technol. **19,** 1352–1365 (2001).
16. T. J. Eom, S.-J. Kim, T.-Y. Kim, C.-S. Park, U.-C. Paek, and B. H. Lee, "Realization of true-time-delay using cascaded long-period fiber gratings: theory and applications to the optical pulse multiplication and temporal encoder/decoder," J. Lightwave Technol. **23,** 597–608 (2005).
17. A. Grunnet-Jepsen, A. E. Johnson, E. S. Maniloff, T. W. Mossberg, M. J. Munroe, and J. N. Sweetser, "Fiber Bragg grating based spectral encoder/decoder for lightwave CDMA," Electron. Lett. **35,** 1096–1097 (1999).
18. S. Zahedi and J. A. Salehi, "Analytical comparison of various fiber-optic CDMA receiver structures," J. Lightwave Technol. **18,** 1718–1727 (2000).
19. X. Wang and K. Kitayama, "Analysis of beat noise in coherent and incoherent time-spreading OCDMA," J. Lightwave Technol. **22,** 2226–2235 (2004).
20. B. Ni and J. S. Lehnert, "Performance of an incoherent temporal spreading OCDMA system with broadband light sources," J. Lightwave Technol. **23,** 2206–2214 (2005).
21. L. Tancevski and L. A. Rush, "Impact of beat noise on the performance of 2D optical CDMA systems," IEEE Commun. Lett. **4,** 264–266 (2000).
22. M. Rochette and L. A. Rusch, "Spectral efficiency of OCDMA systems with coherent pulsed sources," J. Lightwave Technol. **23,** 1033–1038 (2005).
23. S. V. Maric, "New family of algebraically design optical orthogonal codes for use in CDMA fiber optic networks," Electron. Lett. **29,** 538–539 (1993).
24. S. V. Maric, Z. I. Kostic, and E. L. Titlebaum, "A new family of optical code sequences for use in spread-spectrum fiber optic local area networks," IEEE Trans. Commun. **41,** 1217–1221 (1993).
25. Z. Wei, H. M. H. Shalaby, and H. Ghafouri-Shiraz, "Modified quadratic congruence codes for fiber Bragg-grating-based spectral-amplitude-coding optical CDMA systems," J. Lightwave Technol. **19,** 1274–1281 (2001).
26. D. Z. Anderson, V. Mizuehi, T. Erdogan, and A. E. White, "Production of in-fiber gratings using a diffractive optical element," Electron. Lett. **29,** 566–568 (1993).
27. I. Fsaifes, C. Lepers, A.-F. Obaton, and P. Gallion, "DS-OCDMA encoder/decoder performance analysis using optical low coherence reflectometry," J. Lightwave Technol. **24,** 3121–3128 (2006).
28. A. D. Kersey, M. A. Davis, H. J. Patrick, M. LeBlanc, K. P. Koo, C. G. Askins, M. A. Putnam, and E. J. Friebele, "Fiber grating sensors," J. Lightwave Technol. **15,** 1442–1463 (1997).
29. H. Fathallah and L. A. Rusch, "Robust optical FFH-CDMA communications: coding in place of frequency and temperature controls," J. Lightwave Technol. **17,** 1284–1293 (1999).
30. I. Fsaifes, C. Lepers, M. Lourdiane, R. Gabet, and P. Gallion, "Pulsed laser source coherence time impairments in a direct detection DS-OCDMA system," Conference on Lasers and Electro-Optics (2006), paper CWH6.